LOGY

- Rolling Resistance as Derived from Fuel Economy
- Rolling Resistance Measurements of New and Retreaded Truck
- Effect in Rolling Resistance of Highway Truck Tires,
- Effect of Tire Geometry on the Rolling Efficiency of
- SAE 930140.
- L., "Comparison of Laboratory and On-going Truck
- Tread Depths," SAE Paper No. 880584.
- Economy Measurement Study Report, 1975, p. 59.
- Heavy Truck Tires, SAE SP-546.
- for Passenger Car Tires — SAE J1269" and "Tire
- Resistance — SAE J1270," SAE Handbook.
- C. A., and Warolin, T. C., "Interlaboratory Rolling
- Bias Tires," SAE Paper No. 821265 (also published
- Tires, SAE SP-546).
- Gross, D. L., "The Structure and Use of the GMR
- Loss Model," SAE Paper No. 810164.
- Tire Deformation for Power Loss Calculations," SAE
- Dissipation for Power Loss Calculations," SAE Paper
- Affecting The Thermal State of Tires for Power Loss
- Power Loss Modeling," General Motors Research
- 3310, May 30, 1980) and *The General Problem of*
- published by the ASME.
- Tire Treat the Finite Element Analysis of a Statically
- Akron, 1987 (available from University Microfilms).
- Radbert, H., "A Material Model for Simulating the
- Steel Tires," *Tire Science and Technology*, TSTCA,
- 152–68.
- G. L., "RPA Measurement of Hysteresis for CAE
- Paper No. 30A.
- H., "Tire Rolling Loss Computation with the Finite
- Energy," TSTCA, Vol. 22, No. 4, October–December
- Empirical Model for the Transient Rolling Resistance
- Cooling," TSTCA, Vol. 27, No. 3, July–September
- Surface Texture on Tire Rolling Resistance," SAE
- Loading Factor for Truck Tire Rolling Resistance,"

M. Koishi[1] *and S. Govindjee*[2]

Inverse Design Methodology of a Tire[3]

REFERENCE: Koishi, M. and Govindjee, S., "**Inverse Design Methodology of a Tire,**" *Tire Science and Technology*, TSTCA, Vol. 29, No. 3, July–September 2001, pp. 155–170.

ABSTRACT: Most rubber components usually suffer large deformation, thus one should consider finite deformation theories when designing rubber products such as tires. Although finite element analysis (FEA) is useful for computing nonlinear structural response in standard problems, it is more difficult to predict the undeformed original to-be-manufactured shape of a part corresponding to a design constraint involving a prescribed deformed shape under a given load. For example, one can use an optimization technique to predict the original shape in the sense of an inverse problem via successive iteration. As another procedure to solve such inverse problems, Govindjee and Mihalic [4,5] have proposed a new computational procedure to predict undeformed (to-be-manufactured) shapes for prescribed exterior deformed configurations, Cauchy tractions and displacement boundary conditions. In this paper, we demonstrate applications of the inverse shape determination problem for a tire design. The proposed methodology enables us to predict an undeformed (to-be-manufactured) tire shape corresponding to the design constraint of a prescribed exterior deformed configuration. After reviewing the formulation of the inverse shape determination, some numerical examples illustrating the methodology in a tire design are presented.

KEY WORDS: inverse problem, tire design, finite element model (FEM), thermoelasticity

Since most rubber components usually suffer large deformations, we consider finite deformation theories under normal loading conditions when designing rubber products such as tires. In such design, it is often advantageous to consider inverse problem statements where the given information concerns the mechanically and thermally loaded part — for instance, its deformed shape. Finite element analysis (FEA) has been used widely to predict nonlinear responses of tires in tire engineering. Although FEA is useful to compute nonlinear structural responses in the standard (forward) problems, it is difficult to predict the undeformed (to-be-manufactured) original shapes corresponding to the design constraints just mentioned. One possible solution is to use an optimization technique that refines the initial configuration until a standard (forward) computation gives a deformed configuration sufficiently close to the desired deformed

[1] The Yokohama Rubber Co., Ltd., 2-1 Oiwake, Hiratsuka, Kanagawa, 254-8601, Japan.
[2] Department of Civil Engineering, University of California, Berkeley, CA 94720.
[3] Presented at the nineteenth annual conference of The Tire Society, Akron, Ohio, April 25–26, 2000.

shape. By means of such an optimization technique one can predict the original shape of a nonlinear structure in the sense of an inverse problem. Recently, this issue has been seen to be important as the response surface methodology has been recognized as a practical optimization tool in the design process of production models, such as the crash safety design of vehicles [*1,2*] in which highly non-linear FEA is conducted. Further, a shape design methodology of tires has recently been proposed using an optimization technique based on the response surface methodology [*3*]. As an alternative solution method to the inverse problem, Govindjee and Mihalic have proposed a new computational procedure to predict an undeformed shape corresponding to a prescribed exterior deformed configuration, Cauchy traction field and displacement boundary conditions [*4,5*]. This method provides a direct means to satisfy the shape optimization objective without iteration on a series of standard (forward) computations. In contrast to other inverse problems, the inverse deformation problem proposed by them can be "well-posed" in accordance with Hadamard's definition.

In this paper, we demonstrate applications of the inverse shape determination problem for a tire design. The proposed methodology enables us to predict an undeformed tire shape corresponding to the prescribed exterior deformed configuration, Cauchy traction field and displacement boundary conditions. No remeshing techniques and no additional iterations in an optimization process are required in the procedure. The solution comes from the solution of a single equilibrium boundary value problem that has been parameterized in terms of the inverse deformation of the part. Moreover, design variables and objective functions are not also required for the inverse problem description which greatly simplifies problem setup. The mixed finite element formulation of the inverse problem proposed by Govindjee and Mihalic [*4,5*] has been recently extended by Govindjee [*6*] to make it more applicable to tire design analysis; i.e. it has been extended to include thermoelasticity, orthotropic nonlinear elasticity and axis-symmetry. For the present paper, an element has been implemented based on these new developments. After reviewing the formulation of the inverse shape determination problem, some numerical examples are presented as applications of the methodology to a tire design.

Inverse Shape Determination Problem

In this section we outline the problem description on inverse shape determination. In the standard (forward) problem one considers a reference placement of a continuum body $\Omega \subset \mathbb{R}^3$ and its motion ϕ: $\Omega \subset \mathbb{R}^3 \rightarrow \mathbb{R}^3$. Points in the reference placement are denoted by $\mathbf{X} \in \phi$ and map to points $\mathbf{x} = \phi(\mathbf{X})$ in the deformed configuration $\omega = \phi(\Omega)$.

In the standard forward problem the motion $\phi(\mathbf{X})$ is considered the primary unknown when the body is subjected to known boundary displacements and tractions. The motion ϕ is determined by solving the equilibrium equations. The

problem of interest here is the inverse of this problem where the deformed configuration and boundary conditions are known and the reference configuration and inverse motion $\varphi(\mathbf{x}) = \phi^{-1}(\mathbf{X})$ are the desired unknowns. Note, in the specification of the deformed configuration one only needs to specify the region of space that the deformed part occupies: thus really one only specifies exterior or boundary data.

In the standard problem, defining the deformation gradient

$$\mathbf{F} = \frac{\partial \phi}{\partial \mathbf{X}}$$

leads to the relation for the first Piola-Kirchhoff stress tensor

$$\mathbf{P} = \frac{\partial W(\mathbf{F})}{\partial \mathbf{F}}$$

The strong form of equilibrium equations in the standard problem is given by

$$\mathrm{DIV}\,[\mathbf{P}] + \hat{\mathbf{B}} = \mathbf{0} \quad \text{and} \quad \mathbf{F}\mathbf{P}^T = \mathbf{P}\mathbf{F}^T \qquad \forall\, \mathbf{X} \in \Omega$$

$$\mathbf{P}\mathbf{N} = \bar{\mathbf{T}} \qquad \forall\, \mathbf{X} \in \partial\Omega_t$$

$$\phi = \bar{\phi} \qquad \forall\, \mathbf{X} \in \partial\Omega_\phi$$

where $\mathrm{DIV}\,[\,\cdot\,]$ is the divergence operator with respect to $\mathbf{X}$, $\hat{\mathbf{B}}$ is a given body force per unit reference volume, $\bar{\mathbf{T}}$ is a given traction per unit reference area, $\bar{\phi}$ is a given motion, $\partial\Omega_t \cap \partial\Omega_\phi = \varnothing$, and $\partial\Omega_t \cup \partial\Omega_\phi = \partial\Omega$ the boundary of Ω. The unknown of the problem is the forward motion.

On the other hand, the equilibrium equations and boundary conditions in terms of the Cauchy stress $\boldsymbol{\sigma}$ and the known deformed configuration ω for the inverse problem are given by

$$\mathrm{div}\,[\boldsymbol{\sigma}] + \hat{\mathbf{b}} = \mathbf{0} \quad \text{and} \quad \boldsymbol{\sigma} = \boldsymbol{\sigma}^T \qquad \forall\, \mathbf{x} \in \omega$$

$$\boldsymbol{\sigma}\mathbf{n} = \bar{\mathbf{t}} \qquad \forall\, \mathbf{x} \in \partial\omega_t$$

$$\varphi = \bar{\varphi} \qquad \forall\, \mathbf{x} \in \partial\omega_\phi$$

where $\mathrm{div}\,[\,\cdot\,]$ is the divergence operator with respect to $\mathbf{x}$, $\hat{\mathbf{b}}$ is a given body force per unit spatial volume of the deformed body, $\bar{\mathbf{t}}$ is a given traction per unit spatial area on the deformed body, $\bar{\varphi}$ is a given motion, $\partial\omega_t \cap \partial\omega_\phi = \varnothing$, and $\partial\omega_t \cup \partial\omega_\phi = \partial\omega$ the boundary of ω.

Thermoelasticity

Due to the realities of rubber part manufacturing and part usage, we need to consider the thermoelastic deformation of a tire after a cure process; this is especially important in a truck and bus tire design.

If one assumes for simplicity a constant heat capacity, then the Helmholtz free energy function can be expressed as

$$\psi(\mathbf{F}, T) = \frac{T}{T_0}\psi_0(\mathbf{F}) + \left(1 - \frac{T}{T_0}\right)e_0(\mathbf{F}) + \bar{c}\left(T - T_0 - T\ln\frac{T}{T_0}\right) \tag{1}$$

where $\mathbf{F}$ is the deformation gradient, T is the current absolute temperature, T_0 is a reference absolute temperature, ψ_0 is the free energy at T_0, e_0 is the internal energy at T_0, and $\bar{c}$ is the heat capacity. In the special case where one has a separable free energy function for volumetric and deviatoric behavior then Eq 1 is specialized to

$$\psi(\mathbf{F}, T) = \frac{T}{T_0}W_0(\bar{\mathbf{F}}) + \frac{T}{T_0}U_0(J) + \left(1 - \frac{T}{T_0}\right)e_0(J) + \bar{c}\left(T - T_0 - T\ln\frac{T}{T_0}\right) \tag{2}$$

where $J = \det[\mathbf{F}]$ is the Jacobian determinant, $\bar{\mathbf{F}} = J^{-1/3}\mathbf{F}$ is the volume preserving part of the deformation gradient, W_0 is the deviatoric free energy at T_0, and U_0 is the volumetric free energy at T_0.

Isotropic Thermoelasticity

As a particular example of the general setting outlined in the previous section, we consider the case of the regularized neo-Hookean material. Appropriate choices for the function in Eq 2 are

$$W_0(\bar{\mathbf{F}}) = \frac{\mu}{2}(\bar{\mathbf{F}}:\bar{\mathbf{F}} - 3)$$

$$U_0(J) = \frac{\kappa}{4}(J^2 - 2\ln(J) - 1)$$

$$e_0(J) = 3\kappa\alpha T_0 \ln(J)$$

where μ is the shear modulus, κ is the bulk modulus, and α is the coefficient of thermal expansion. The corresponding Cauchy stress tensor is given as

$$\sigma = \frac{T}{T_0}\frac{\mu}{J}\operatorname{dev}[\bar{\mathbf{b}}] + \left[\frac{T}{T_0}\frac{\kappa}{2}\left(J - \frac{1}{J}\right) + (T_0 - T)3\kappa\alpha\frac{1}{J}\right]\mathbf{1} \tag{3}$$

where $\operatorname{dev}[\cdot] = (\cdot) - \frac{1}{3}(\mathbf{1}:(\cdot))\mathbf{1}$, and $\bar{\mathbf{b}} = \bar{\mathbf{F}}\bar{\mathbf{F}}^T$. If we express Eq 3 in terms of the inverse motion then one has

$$\boldsymbol{\sigma} = \frac{T}{T_0}\mu j \,\mathrm{dev}\,[\bar{\mathbf{c}}^{-1}] + \left[\frac{T}{T_0}\frac{\kappa}{2}\left(\frac{1}{j} - j\right) + (T_0 - T)3\kappa\alpha j\right]\mathbf{1}$$

where $j = 1/J$, $\mathbf{c} = \mathbf{f}^T\mathbf{f}$ and $\bar{\mathbf{f}} = \bar{\mathbf{F}}^{-1}$. For convenience split the stress as $\boldsymbol{\sigma} = \mathbf{s} + p\mathbf{1}$ so that the deviatoric stress

$$\mathbf{s} = \frac{T}{T_0}\mu j \,\mathrm{dev}\,[\bar{\mathbf{c}}^{-1}]$$

and the pressure

$$p = \hat{p}(j) = \frac{T}{T_0}\frac{\kappa}{2}\left(\frac{1}{j} - j\right) + (T_0 - T)3\kappa\alpha j$$

Orthotropic Thermoelasticity

To model reinforcements in a tire, special reinforcement elements have been developed in the past and implemented in some commercial FEA codes [7]. Here, we implement the finite elastic constitutive model for fiber-reinforced materials given by Spencer [8] in terms of two orthogonal material director vectors $\mathbf{P}$ and $\mathbf{Q}$.

The free energy is taken as an orthotropic Saint-Venant Kirchhoff material model given by

$$\Psi_0 = \tfrac{1}{2}\lambda I_1^2 + \mu I_2 + (\alpha_1 I_4 + \alpha_2 I_6)I_1 + 2\mu_1 I_5 + 2\mu_2 I_7 + \tfrac{1}{2}\beta_1 I_4^2 + \tfrac{1}{2}\beta_2 I_6^2 + \beta_3 I_4 I_6$$

where the invariants can be defined as $I_1 = \mathrm{tr}\,[\mathbf{E}]$, $I_2 = \mathbf{E}{:}\mathbf{E}$, $I_3 = \mathrm{tr}\,[\mathbf{E}^3]$, $I_4 = \mathbf{P}{:}\mathbf{E}{:}\mathbf{P}$, $I_5 = \mathbf{P}{:}\mathbf{E}^2{:}\mathbf{P}$, $I_6 = \mathbf{Q}{:}\mathbf{E}{:}\mathbf{Q}$ and $I_7 = \mathbf{Q}{:}\mathbf{E}^2{:}\mathbf{Q}$. Then, λ, μ, α_1, α_2, μ_1, μ_2, β_1, β_2 and β_3 are elastic constants and $\mathbf{E}$ denotes Green-Lagrange strain tensor.

The inclusion of thermal effects required the specification of the internal energy. To allow for orthotropic thermal expansion there must be three coefficients of thermal expansion in the three orthogonal directions. An appropriate expansion for the internal energy is given by

$$e_0 = \alpha_p T_0[(\alpha_1 + \beta_1 + 2\mu + 4\mu_1)I_4 + (\alpha_2 + \beta_3)I_6 + (\lambda + \alpha_1)I_1] + \alpha_q T_0[(\alpha_2 + \beta_2 + 2\mu + 4\mu_2)I_6 + (\alpha_1 + \beta_3)I_4 + (\lambda + \alpha_2)I_1] + \alpha_r T_0[(\lambda + 2\mu)I_1 + (\alpha_1 - 2\mu)I_4 + (\alpha_2 - 2\mu)I_6]$$

The above constants are related to the entries in the conventional stiffness matrix as follows when the $\mathbf{P}$ and $\mathbf{Q}$ directions line up with the 1- and 2-coordinate directions.

$$\mathbb{D} = \begin{bmatrix} \lambda + 2\alpha_1 + \beta_1 + 2\mu + 4\mu_1 & \lambda + \alpha_1 + \alpha_2 + \beta_3 & \lambda + \alpha_3 & 0 & 0 & 0 \\ & \lambda + 2\alpha_2 + \beta_2 + 2\mu + 4\mu_2 & \lambda + \alpha_2 & 0 & 0 & 0 \\ & & \lambda + 2\mu & 0 & 0 & 0 \\ & & & \mu + \mu_1 & 0 & 0 \\ & & & \mu_2 & & \\ & \text{Symm.} & & & \mu + \mu_2 & 0 \\ & & & & & \mu + \mu_3 \end{bmatrix}$$

This leads to the Cauchy stress being expressible in terms of the inverse motion as

$$\begin{aligned} \boldsymbol{\sigma} = j\Bigg[\Bigg\{\Bigg(\lambda i_1 - \alpha_1 \frac{i_4}{\hat{i}_4} - \alpha_2 \frac{i_6}{\hat{i}_6}\Bigg)\mathbf{c}^{-1} + \Bigg(\alpha_1 i_1 - \beta_1 \frac{i_3}{\hat{i}_3} - \beta_3 \frac{i_6}{\hat{i}_6}\Bigg)\frac{1}{\hat{i}_4}\mathbf{p} \otimes \mathbf{p} + \Bigg(\alpha_2 i_1 \\ - \beta_2 \frac{i_6}{\hat{i}_6} - \beta_3 \frac{i_3}{\hat{i}_3}\Bigg)\frac{1}{\hat{i}_6}\mathbf{q} \otimes \mathbf{q} + 2\mu\mathbf{c}^{-1}\boldsymbol{\varepsilon} + 2\mu_1 \frac{1}{\hat{i}_4}(\mathbf{p} \otimes \boldsymbol{\varepsilon}\mathbf{p} + \boldsymbol{\varepsilon}\mathbf{p} \otimes \mathbf{p}) \\ + 2\mu_2 \frac{1}{\hat{i}_6}(\mathbf{q} \otimes \boldsymbol{\varepsilon}\mathbf{q} + \boldsymbol{\varepsilon}\mathbf{q} \otimes \mathbf{q})\Bigg\}\frac{T}{T_0} + (T_0 - T)\{\alpha_p(\alpha_1 + \beta_1 + 2\mu + 4\mu_1) \\ + \alpha_q(\alpha_1 + \beta_3) + \alpha_r(\alpha_1 - 2\mu)\}\frac{1}{\hat{i}_4}\mathbf{p} \otimes \mathbf{p} \\ + (T_0 - T)\{\alpha_q(\alpha_2 + \beta_2 + 2\mu + 4\mu_2) + \alpha_p(\alpha_2 + \beta_3) \\ + \alpha_r(\alpha_2 - 2\mu)\}\frac{1}{\hat{i}_6}\mathbf{p} \otimes \mathbf{p} + (T_0 - T)\{\alpha_p(\lambda + \alpha_1) \\ + \alpha_q(\lambda + \alpha_2) + \alpha_r(\lambda + 2\mu)\}\mathbf{c}^{-1}\Bigg] \end{aligned}$$

where

$$i_1 = \operatorname{tr}[\boldsymbol{\varepsilon}]$$

$$i_4 = (\mathbf{p} \otimes \mathbf{p}):\boldsymbol{\varepsilon} \qquad i_6 = (\mathbf{q} \otimes \mathbf{q}):\boldsymbol{\varepsilon}$$

$$\hat{i}_4 = (\mathbf{p} \otimes \mathbf{p}):\mathbf{c} \qquad \hat{i}_6 = (\mathbf{q} \otimes \mathbf{q}):\mathbf{c}$$

$$\boldsymbol{\varepsilon} = \frac{1}{2}(\mathbf{c}^{-1} - \mathbf{1}) \qquad \mathbf{e} = \frac{1}{2}(\mathbf{c} - \mathbf{1})$$

$$\mathbf{P} = \frac{\mathbf{fp}}{\|\mathbf{fp}\|} \qquad \text{and} \qquad \mathbf{P} \cdot \mathbf{fq} = 0$$

INOLOGY

$$\begin{bmatrix} \lambda - \alpha_1 & 0 & 0 & 0 \\ + \beta_1 & & & \\ + \beta_2 & \lambda - \alpha_2 & 0 & 0 \\ + 4\mu_2 & & & \\ & \lambda - 3\mu & 0 & 0 \\ & & \mu + \mu_1 & 0 \\ & & \mu_2 & \\ & & & \mu + \mu_1 \end{bmatrix}$$

ing expressible in terms of the inverse motion

$$+ \left(\alpha_2 i_3 - \beta_1 \frac{i_2}{i_3} - \beta_2 \frac{i_3^2}{i_3} \right) \frac{1}{i_3} \mathbf{p} \otimes \mathbf{p} + \left(\alpha_2 i_1 \right.$$

$$+ 2\mu \mathbf{c}^{-1}\boldsymbol{\epsilon} - 2\mu_1 \frac{1}{i_3} (\mathbf{p} \otimes \boldsymbol{\epsilon}\mathbf{p} - \boldsymbol{\epsilon}\mathbf{p} \otimes \mathbf{p})$$

$$) \mathbf{q}) \left\{ \frac{T}{T_0} - (T_0 - T)[\alpha_2(\alpha_2 + \beta_1 + 2\mu + 4\mu_1) \right.$$

$$2\mu_2)\} \frac{1}{i_3} \mathbf{p} \otimes \mathbf{p}$$

$$+ \mu_1 + 4\mu_2) + \alpha_2(\alpha_2 + \beta_2)$$

$$+ (T_0 - T)[\alpha_2(\lambda + \alpha_1)$$

$$\left. - \alpha_2(\lambda - \alpha_2) + \alpha_1(\lambda + 2\mu)\} \mathbf{c}^{-1} \right]$$

$$i_2 = \mathrm{tr}[\boldsymbol{\epsilon}]$$

$$\mathbf{p}):\mathbf{e} \qquad i_3 = i(\mathbf{q} \otimes \mathbf{q}):\mathbf{e}$$

$$\mathbf{p}):\mathbf{c} \qquad i_4 = i(\mathbf{q} \otimes \mathbf{q}):\mathbf{c}$$

$$- 1) \qquad \mathbf{e} = \frac{1}{2}(\mathbf{c} - \mathbf{1})$$

and $\quad \mathbf{F} \cdot \mathbf{f}\mathbf{q} = \mathbf{0}$

Inverse Three Field Finite Element Formulation

To satisfy incompressibility of rubber materials the three field weak formulation of Simo and Taylor [9] is used in conjunction with the above model. The corresponding weak form equations are given by

$$G_\theta(\varphi, \theta; \beta) = \int_\omega [j - \theta]\beta = 0$$

$$G_p(\theta, p; \alpha) = \int_\omega [\hat{p}(\theta) - p]\alpha = 0$$

and

$$G_\varphi(\varphi, p; \boldsymbol{\eta}) = \int_\omega [\mathbf{s}:\mathrm{grad}\,(\boldsymbol{\eta}) + p\,\mathrm{div}\,(\boldsymbol{\eta})] + G_{ext} = 0$$

where the variations are such that $\boldsymbol{\eta}$: $\boldsymbol{\omega} \to \mathbf{R}^3$ and $\boldsymbol{\eta} = \mathbf{0}$ on $\partial\omega_\varphi$, β: $\omega \to \mathbf{R}$, α: $\omega \to \mathbf{R}$ and G_{ext} contains the contribution of the tractions and body forces: θ is the mixed Jacobian.

If constant approximations per element for β, α, θ and p are assumed then the linearization of above weak form equations gives the needed tangential operator for non-linear FEA computation as

$$D_1 G_\varphi(\varphi; \boldsymbol{\eta})[\mathbf{v}] = \int_{\omega_e} \mathrm{sym}\,[\mathrm{grad}\,(\boldsymbol{\eta})]:\left[2\frac{\partial \mathbf{s}}{\partial \mathbf{c}}\right]:\mathrm{sym}\,[\mathbf{f}^T\,\mathrm{grad}\,(\mathbf{v})]$$

$$+ \left(\int_{\omega_e} \mathrm{div}\,(\boldsymbol{\eta})\right) \frac{d\hat{p}(\theta)/d\theta}{v_e} \left(\int_{\Omega_e} \mathrm{DIV}\,(\mathbf{v})\right)$$

where v_e is the spatial volume of an element. For the isotropic model at hand we have that

$$\frac{d\hat{p}}{d\theta}(\theta) = \frac{T}{T_0}\frac{\kappa}{2}\left(-\frac{1}{\theta^2} - 1\right) + (T_0 - T)3\kappa\alpha$$

And

$$\frac{\partial \mathbf{s}}{\partial \mathbf{c}} = \mu \frac{T}{T_0} j^{1/3}\left[\frac{5}{6}\,\mathrm{dev}\,[\bar{\mathbf{c}}^{-1}] \otimes \bar{\mathbf{c}}^{-1} - \mathbf{I}_{\bar{c}^{-1}} + \frac{1}{3}\mathbf{1} \otimes \bar{\mathbf{c}}^{-2}\right]$$

where $\bar{\mathbf{c}} = \bar{\mathbf{f}}^T\bar{\mathbf{f}}$, $\bar{\mathbf{f}} = j^{-1/3}\mathbf{f}$, and $[\mathbf{I}_{\bar{c}^{-1}}]_{ijkl} = \frac{1}{2}(\bar{c}^{-1}_{ik}\bar{c}^{-1}_{jl} + \bar{c}^{-1}_{il}\bar{c}^{-1}_{jk})$.

An axis-symmetric finite element of the above models has been implemented for inverse shape determination of a tire subjected to axis-symmetric finite deformation including thermal effects; see Govindjee [6] for additional implementational details.

Numerical Examples

Rubber Column under Prescribed Compression

In the first example, we demonstrate the effectiveness of the above formulation by comparing it with a quasi-inverse method that is used in conjunction with the standard (forward) solution procedure from ABAQUS [7]. The quasi-inverse method refers to a simple reversal of boundary tractions and displacements and is a way to predict undeformed shapes by standard FEA. We note however that this is strictly valid only in the linear setting and our computations, shown below, demonstrate this fact. Figure 1 shows the undeformed shape of a rubber column, which has height of 20 mm and radius of 10 mm. Material properties are κ = 166.7 MPa and μ = 35.7 MPa. The top surface is subjected to prescribed displacements that generate a compressive strain of 40%; the bottom surface is clamped. Figure 2 shows an initial finite element mesh, which models a half cross-section due to symmetry. The deformed shape obtained by a standard (forward) computation is shown in Fig. 3 in which the deformed shape is plotted in 3D as a 270 degrees wedge. We use this spatial configuration from the forward solution as the initial configuration for an inverse computation. As such, we have a known undeformed shape against which to test inverse methods. Figure 4 shows the calculated undeformed shape by means of the proposed procedure. The resulting shape corresponds completely with the initial configuration shown in Fig. 1. The inverse solution is found to be accurate to 4 significant digits with respect to the forward solution. On the other hand, the same accuracy is not obtained by the quasi-inverse method used in conjunction with ABAQUS as is shown in Fig. 5 where elements near the top surface are distorted. This numerical

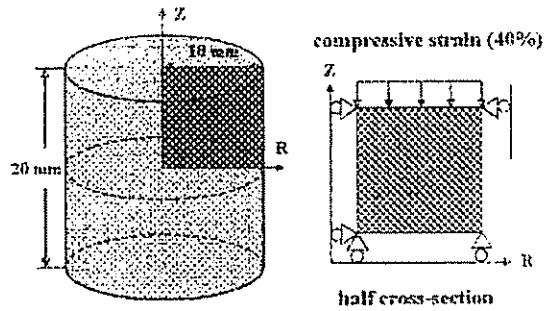

FIG. 1 — *Rubber column under prescribed compression.*

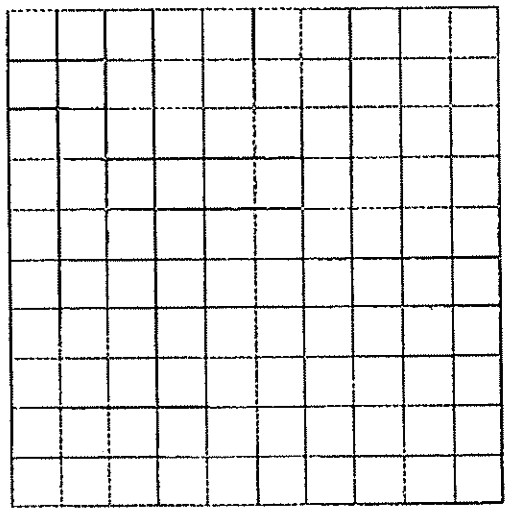

FIG. 2 — *Finite element mesh of half cross-section of rubber column.*

example shows in part the effectiveness and accuracy of the proposed procedure for an axis-symmetric problem.

Post Cure Inflation of a Passenger Car Tire

A shape design of a passenger car radial tire sized 195/65R15 is considered in the present numerical example. Figure 6 shows the finite element model of an initial layout of a cured tire. This FE model has 253 nodes and 214 elements. The material properties for a post cure inflation process are used which account for high temperature effects. In order to have an inverse problem with a known solution for error checking, the deformed shape is computed by standard FEA under a post cure inflation pressure of 200 kPa; see Fig. 7 with initial layout. The resulting deformed shape is now utilized as a desired deformed shape in this

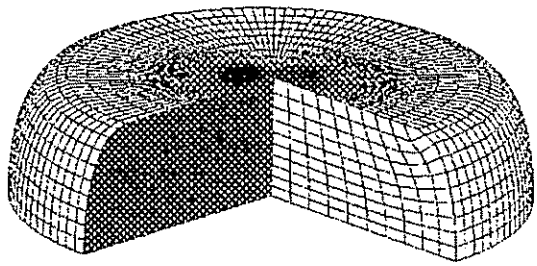

FIG. 3 — *Deformed configuration calculated by standard FEA.*

OLOGY

of the above models has been implemented a tire subjected to axis-symmetric finite ; see Govindjee [6] for additional imple-

ompression

the effectiveness of the above formulation method that is used in conjunction with the re from ABAQUS [7]. The quasi-inverse boundary tractions and displacements and es by standard FEA. We note however that setting and our computations, shown below, s the undeformed shape of a rubber column, ius of 10 mm. Material properties are κ = The top surface is subjected to prescribed essive strain of 40%; the bottom surface is finite element mesh, which models a half deformed shape obtained by a standard ig. 3 in which the deformed shape is plotted e this spatial configuration from the forward as an inverse computation. As such, we have which to test inverse methods. Figure 4 e by means of the proposed procedure. The dy with the initial configuration shown in 4 to be accurate to 4 significant digits with the other hand, the same accuracy is not d used in conjunction with ABAQUS as is the top surface are distorted. This numerical

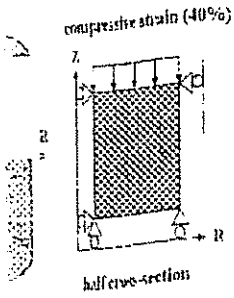

under prescribed compression.

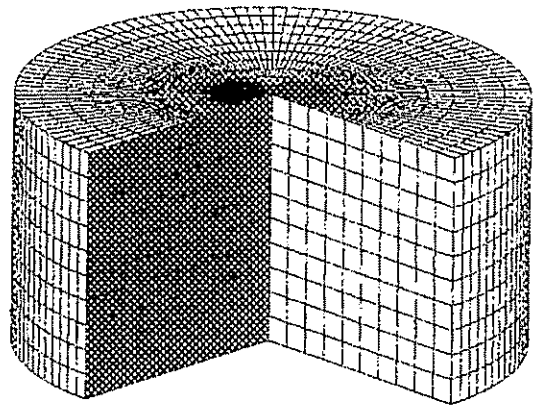

FIG. 4 — *Resulting undeformed shape calculated by proposed procedure.*

example. Before starting inverse shape determination we also demonstrate the accuracy of the developed FE program in the forward sense. Figure 8 shows a comparison of the deformed shape by ABAQUS and the developed FE program. This figure shows the appropriateness of the developed code for also computing the static nonlinear response of a tire. To demonstrate the effectiveness of the proposed procedure, the quasi-inverse solution calculated using ABAQUS is shown in Fig. 9. In this computation, a converged solution is not obtained. Moreover, buckling can be observed at the sidewall. On the other hand, the undeformed shape computed using the proposed method is shown in Fig. 10 and is seen to correspond well to the initial shape. This inverse solution is the objective layout of the cured tire.

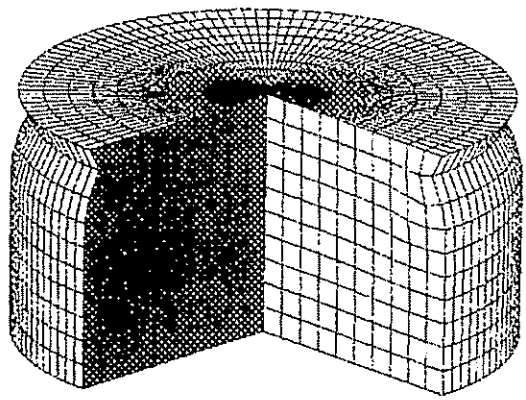

FIG. 5 — *Quasi-inverse solution using ABAQUS.*

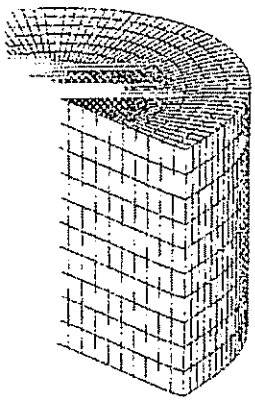

d shape calculated by proposed procedure.

shape determination we also demonstrate the ogram in the forward sense. Figure 8 shows a by ABAQUS and the developed FE program. ess of the developed code for also computing tire. To demonstrate the effectiveness of the verse solution calculated using ABAQUS is ation, a converged solution is not obtained. ved at the sidewall. On the other hand, the the proposed method is shown in Fig. 10 and initial shape. This inverse solution is the

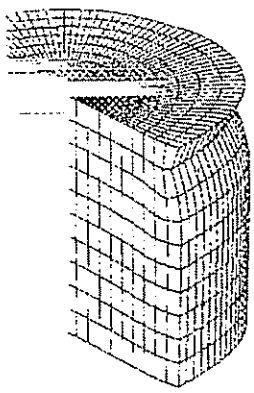

Inverse solution using ABAQUS.

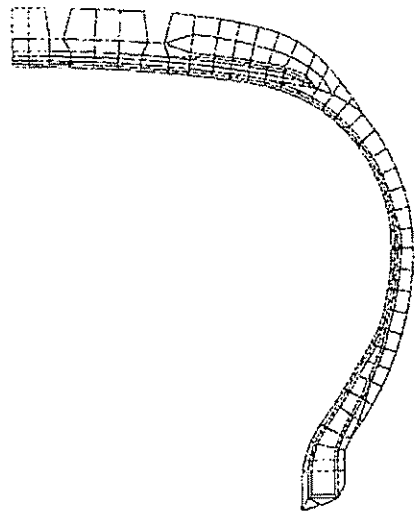

FIG. 6 — *Finite element model of the initial configuration of a 195/65R15 radial tire.*

Layout Determination of a Cured Truck and Bus Tire

In this example we consider the determination of the layout of a cured truck and bus radial tire sized 11R22.5. Figure 11 shows the finite element mesh, which is modeled by 177 nodes and 151 elements of initial layout. First, we compute a

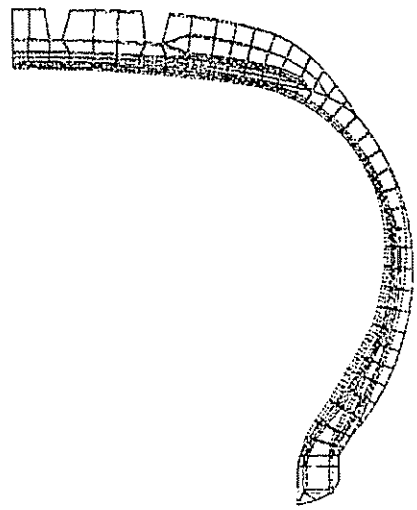

FIG. 7 — *Deformed shape under post cure inflation (solid line) and initial configuration (dash line).*

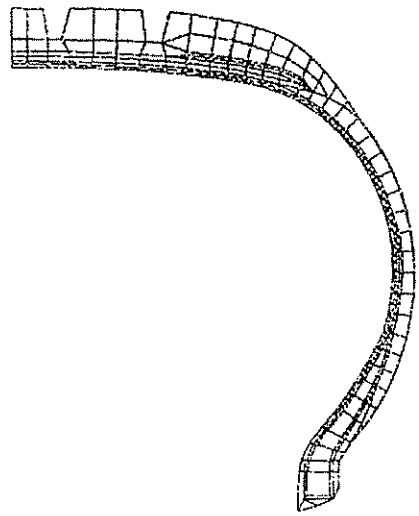

FIG. 8 — *Comparison of forward deformation calculated by developed FEA program (solid line) and with ABAQUS (dash line).*

deformed configuration from this initial design under an inflation pressure of 700 kPa, rim mounting and temperature change. In the deformed state, the temperature is 300 K, and the initial undeformed configuration is at a temperature of 450

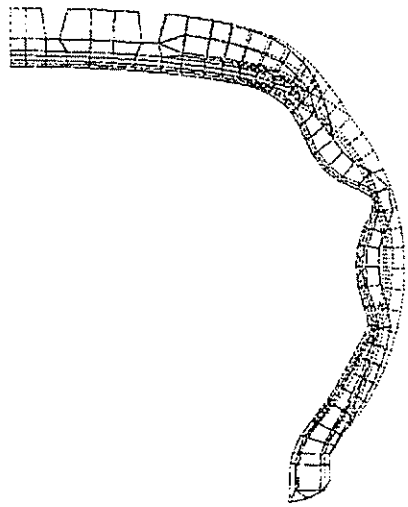

FIG. 9 — *Quasi-inverse solution by ABAQUS (solid line) and initial deformed configuration (dash line).*

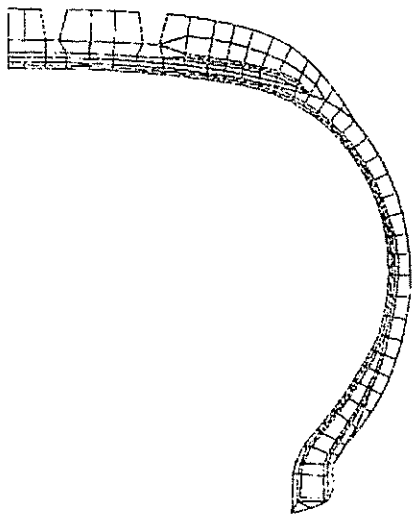

FIG. 10 — *Comparison between resulting undeformed shape by proposed procedure (solid line) and initial undeformed shape (dash line).*

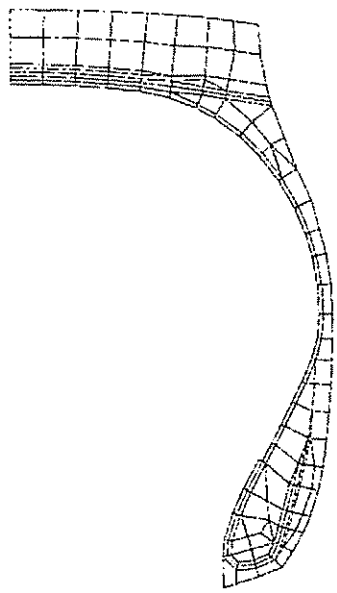

FIG. 11 — *Finite element model of the initial layout of a cured truck and bus tire sized 11R22.5.*

LOGY

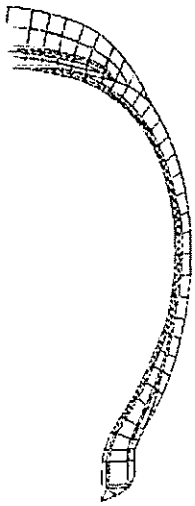

alculated by developed FEA program (solid line) and

=I design under an inflation pressure of 700
hange. In the deformed state, the temper-
ed configuration is at a temperature of 450

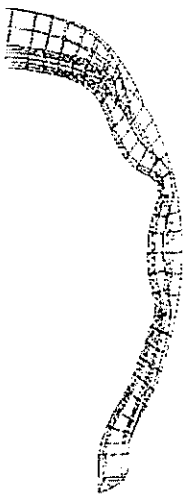

(solid line) and initial deformed configuration (dash

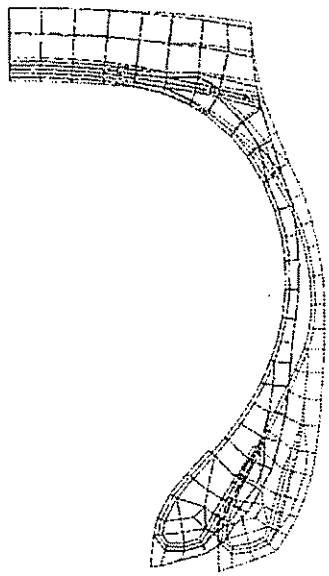

FIG. 12 — *Deformed shape (solid line) and initial shape (dash line).*

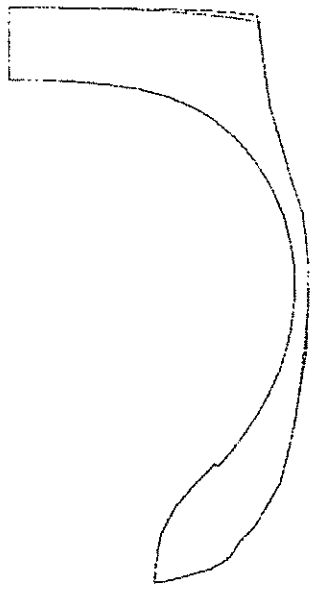

FIG. 13 — *Original deformed shape (dash line) from initial design and desired deformed shape (solid line) in which cap tread and side tread profile are changed.*

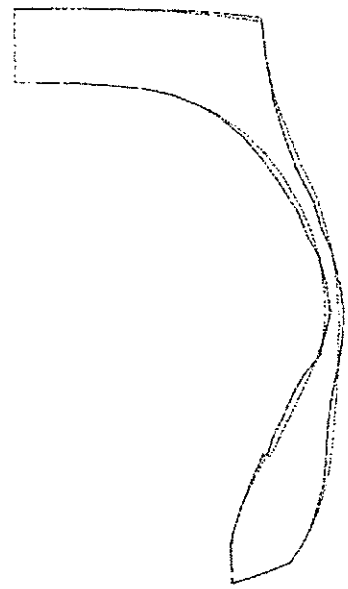

FIG. 14 — *Comparison of the predicted layout (solid line) based on desired deformed shape with the initial design of layout (dash line).*

K. The coefficient of thermal expansion of the rubber is 7.7×10^{-5} and that of the steel wire is 1.2×10^{-5}. This deformed shape is shown in Fig. 12. The thickness of the cap tread thins because of thermoelastic deformation. In the next step, we consider two small design changes on the calculated deformed shape and compute the new initial configuration need for manufacturing. In particular, we alter the deformed profile of the cap tread and side tread as shown in Fig. 13. Figure 14 shows the required undeformed shape as predicted by our inverse shape determination procedure under the given design changes. The resulting undeformed shape is complicated and is not obtained by intuition. To verify this inverse solution, we use it in a standard FEA computation and compare it with the desired deformed shape. The differences of nodal coordinates in such a comparison is found to be less than 0.5%. In this example, although we considered an initial design, we do not need an initial design for the new inverse design procedure. We only need to consider a desired deformed shape under some loading conditions.

Summary

This paper has presented an inverse design methodology of tires in the sense of an inverse problem. Some numerical examples of tire design show the

effectiveness of the proposed procedure. The proposed methodology enables us to design tires considering large deformations under general loading conditions. We only need to consider a desired deformed shape under known loading conditions and we are able to compute to-be-manufactured shapes.

The proposed procedure can also be easily integrated with other numerical design procedures, such as optimization techniques to create advanced tire designs.

References

[1] Yajima, H., Yu, Q., Shiratori, M., and Motoyama, K., "Application of the Statistical Design Support System toward Optimization of Vehicle Safety Equipment," *6th International Conference on Computer Aided Optimum Design of Structures (OPTI '99)*, March 1999, pp. 129–137.

[2] Yu, Q., Yajima, H., Shiratori, M., Motoyama, K., and Yoshimoto, T., "Optimization of Reinforced Members for Crash Safety Design," *6th International Conference on Computer Aided Optimum Design of Structures (OPTI '99)*, March 1999, pp. 355–363.

[3] Nakajima, Y., Kadowaki, H., Kamegawa, T., and Ueno, K., "Application of a Neural Network for the Optimization of Tire Design," *Tire Science and Technology*, TSTCA, Vol. 27, No. 2, April–June 1999, pp. 62–83.

[4] Govindjee, S. and Mihalic, P., "Computational Methods for Inverse Finite Elastostatics," *Computer Methods in Applied Mechanics and Engineering*, Vol. 136, 1996, pp. 47–57.

[5] Govindjee, S. and Mihalic, P., "Computational Methods for Inverse Deformations in Quasi-Incompressible Finite Elasticity," *International Journal for Numerical Methods in Engineering*, Vol. 43, 1998, pp. 821–828.

[6] Govindjee, S., "Finite Deformation Inverse Design Modeling with Temperature Changes, Axis-Symmetry, and Anisotropy," Report No. UCB/SEMM-1999/01, Department of Civil Engineering, University of California Berkeley, 1999.

[7] *ABAQUS/Standard User's Manual V5.8*, Hibbitt, Karlsson & Sorensen, Inc., 1998.

[8] Spencer, A., *Continuum Theory of the Mechanics of Fiber Reinforced Composites*, Springer-Verlag, 1984, pp. 1–32.

[9] Simo, J. and Taylor, R., "Quasi-Incompressible Finite Elasticity in Principal Stretches. Continuum Basis and Numerical Algorithms," *Computer Method in Applied Mechanics and Engineering*, Vol. 85, 1991, pp. 273–310.